8th International Symposium on Magnetic Bearing
August 26-28, 2002, Mito, Japan

COMBINED FORCE/POSITION AND MOMENT/SLOPE CONTROL OF LEVITATED CONTINUA

Xiaodong Lu, Ming-chih Weng, David L. Trumper
Dept. of Mechanical Eng., M.I.T., Cambridge, MA 02139, USA, trumper@mit.edu

ABSTRACT

One of the main challenges in magnetic levitation of flexible structures is the multitude of lightly-damped modes. These modes make it difficult to design a controller which is robustly stable. To address this problem we have developed spatial filtering methods for the magnetic suspension of flexible structures. Some approaches to this have been presented previously [1]. In the present works, we introduce the idea of combining spatially-filtered control loops which operate in parallel on force/position and moment/slope pairs. In the force/position control loop, by taking the averaged output of a sensor array and/or applying an averaged force to an actuator array, "cosine" spatial filters can be created to effectively attenuate undesired resonance modes without adversely affecting the phase of other modes and thus the suspension stiffness will be greatly enhanced. Similarly, in the moment/slope control loop, by taking the difference of the outputs of the position sensor array and/or by applying differential actuating forces to the actuator array, "sinc" spatial filters can be created which change the backbone of the moment/angle dynamics from -20db/decade to -40db/decade, but also to smooth out undesired resonance peaks.

All these spatial filtering effects are analyzed by modal analysis and it is shown that the resulting modal gains are independent of the specific boundary conditions as well as the sensor/actuator set positions relative to the work piece. In this sense, our spatial filtering methods are robust for continua levitation and are thus applicable to a wide range of structural control problems.

In this paper, we present the spatial filtering technique applied to beams. In support of this work, as reported earlier [1], we have constructed a magnetic suspension test bed to control the flexible modes of a 3 m long, 6.35 mm diameter steel tube. The experimental results confirm the value of the averaging techniques, and suggest the wide future application of these ideas in industrial processes which may require non-contact levitating continua.

This work is supported by the National Science Foundation under Grant DMI-9700973.

INTRODUCTION

Levitation of continuum structures may be required in the future in industrial operations, such as steel rolling, plastic film production, paper production, coating, and painting. Non-contact handling by magnetic or electrostatic suspension can be advantageous for these manufacturing processes [2][3][4]. For example, Dr. Conrad Smith [5] developed an idea for the production of painted metal handles for brooms and mops as shown in Fig. 1. The processing steps include forming and seam-welding, powder coating, induction heating, curing, water quenching, and cutting coated tubes into segments. In the sections between the powder coat and the water bath, the 47 m long tube is supported by magnetic suspensions. There are 10 suspension stations, with a spacing of 3 to 4 m between stations. Here the long thin tube results in a rich set of flexible modes. Even in conventional magnetic bearings, when the interested bandwidth is increased to achieve higher performance, flexible modes of the structures will be encountered [6], so the levitated objects are modelled more properly as continua than as lumped-parameter rigid bodies.

The goal of our research is to investigate the vibration control of such levitated continua. In the levitated flexible continua, high resonance peaks will appear, usually with very small damping. These peaks become denser and denser on a logarithmic plot as frequency increases, because the number of resonating modes increase linearly with frequency. There will thus be regions of multiple 0dB crossover by the control loop transmission magnitude. Therefore, a broad range of the frequency response will affect the stability of the closed loop system. A lot of efforts have been made in this area. Temporal notch filters are effective in attenuating the resonance peaks at a specified location, but they are very sensitive to parameter uncertainties [7]. The modal control method [8] extracts modal coordinates and applies modal forces to the vibration modes to be controlled. But the modal control method is model-based and requires the knowledge of the modal shapes, and is thus sensitive to modelling errors.

This research investigates a spatial filtering method. By placing the sensors and actuators in an array, desired spatial filters can be implemented.

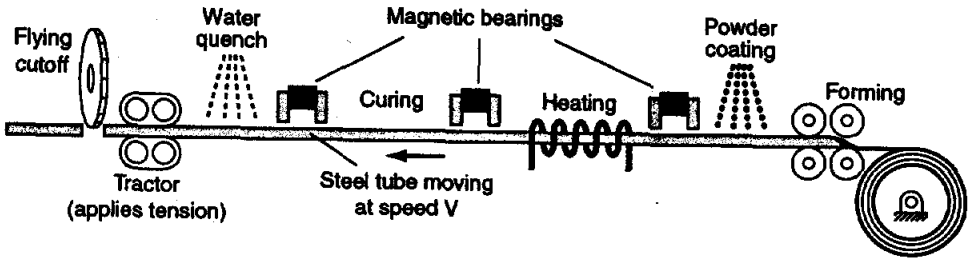

Fig. 1. Non-contact coating process for broom handles, as developed by Smith [4].

These spatial filters will smooth out the high frequency resonating modes without adversely affecting the phase of the low frequency range. Moreover, the benefits from this spatial filtering technique can be easily integrated with other temporal controller design methods(lead-lag, etc).

In an earlier publication [1], an spatial filtering has been demonstrated in the position/force control of levitated continua. While position/force constraints are only one half of the possible degree of freedom, we need to feedback control of both the transverse position and the rotation angle to better constrain the flexible structure. As the backbone of the Bode plot from moment input to slope output is -20db/decade and the phase is very near to $-180°$, it is much more difficult to increase the rotation stiffness than to increase the position stiffness. This paper presents the spatial filtering methods on both force/position and moment/rotation control with more emphasis on the latter.

BEAM MODEL

This section introduces the beam dynamics via modal analysis [9]. The beam without tensional force is represented by the Euler-Bernoulli beam equation

$$EI\frac{\partial^4 u}{\partial z^4} + \rho A\frac{\partial^2 u}{\partial t^2} = f, \qquad (1)$$

where EI is the bending stiffness, u is the transverse deformation, z is the axial dimension, ρA is the mass per unit length, and f is the external transverse force density. The beam vibration is first represented by

$$u(z,t) = \sum_{n=1}^{\infty}\xi_n(t)\phi_n(z). \qquad (2)$$

Similarly, we represent transverse rotation $\theta(z,t)$ by

$$\theta(z,t) = \frac{\partial}{\partial z}u(z,t) = \sum_{n=1}^{\infty}\xi_n(t)\frac{d}{dz}\phi_n(z). \qquad (3)$$

Here $\xi_n(t)$ is the n-th modal coordinate, and $\phi_n(z)$ is the n-th modal shape of beam transverse vibration:

$$\phi_n(z) = (C_{n1}\cos k_n z + C_{n2}\sin k_n z + C_{n3}\cosh k_n z + C_{n4}\sinh k_n z). \qquad (4)$$

The wave number k_n and the modal frequency ω_n are related through the associated beam dispersion equation

$$k_n = \sqrt[4]{\frac{\rho A\omega_n^2}{EI}}. \qquad (5)$$

The constants C_{ni} are determined from boundary conditions. For magnetic suspension of such slender structures, the main control problem is associated with the high-frequency modes. As the evanescent waveforms near the boundaries are less important for these high frequencies, we assume the beam vibration is dominated by the sinusoidal terms and the beam vibration is thus approximated by

$$u(z,t) = \sum_{n=1}^{\infty}\xi_n(t)(C_{n1}\cos k_n z + C_{n2}\sin k_n z). \qquad (6)$$

From the orthogonality properties of each mode, the partial differential equation (1) can be decoupled into infinite number of ordinary differential equations [9]:

$$M_n(\ddot{\xi}_n + 2\zeta_n\omega_n\dot{\xi}_n + \omega_n^2\xi_n) = N_n, \text{ n=1, 2, } \cdots\infty. \qquad (7)$$

where nth modal mass M_n and nth modal force N_n are defined by:

$$M_n = \int_0^L \rho A\phi_n^2 dz, \qquad (8)$$

$$N_n = \int_0^L f\phi_n dz. \qquad (9)$$

For a concentrated force $F(t)$ at z_a, $f = F(t)\delta(z - z_a)$, where δ is the unit impulse, and thus the modal force can be reformulated as:

$$N_n(t) = \int_0^L F(t)\delta(z - z_a)\phi_n(z)dz = F(t)\phi_n(z_a). \qquad (10)$$

For a beam position sensor with output y located at z_s,

$$y(t) = u(z_s, t) = \sum_{n=1}^{\infty} \xi_n(t)\phi_n(z_s). \tag{11}$$

From equations (7) (10) and (11), the transfer function from a concentrated point force F at z_a to a position feedback y at z_s can be derived:

$$\frac{y(s)}{F(s)} = \sum_{n=1}^{\infty} \frac{\phi_n(z_s)\phi_n(z_a)}{M_n(s^2 + 2\zeta_n\omega_n s + \omega_n^2)}. \tag{12}$$

Similarly, for a concentrated moment $T(t)$ at z_a, the force density can be formulated as: $f = -T(t)u_1(z - z_a)$, where $u_1(z)$ is unit doublet function, and thus via integration by parts,

$$\begin{aligned} N_n(t) &= \int_0^L -T(t)u_1(z - z_a)\phi_n(z)dz \\ &= T(t)\frac{d}{dz}\phi_n(z_a). \end{aligned} \tag{13}$$

The beam slope at z_s is given by,

$$\theta(t) = \sum_{n=1}^{\infty} \xi_n(t)\frac{d}{dz}\phi_n(z_s). \tag{14}$$

Thus the transfer function from a concentrated moment T at position z_a to a slope feedback θ at position z_s is:

$$\frac{\theta(s)}{T(s)} = \sum_{n=1}^{\infty} \frac{\frac{d}{dz}\phi_n(z_s)\frac{d}{dz}\phi_n(z_a)}{M_n(s^2 + 2\zeta_n\omega_n s + \omega_n^2)}. \tag{15}$$

For our experimental 3 m long tubular beam, Fig. 2 illustrates the calculated Bode plots of the two transfer functions (12) and (15) with $z_s = z_a = 1$m and with $z_s = z_a = 1.3$m under free-free boundary conditions.

To design controllers to stabilize the beam, we are more concerned with the peak envelope of the Bode plots labelled as the uncertainty envelope in Fig. 2. When the suspended object is moving, thereby shifting the points of force application and sensor feedback relative to the mode structure, the Bode plots will change greatly as shown in Fig. 2, while the uncertainty envelope will remain the same. With assumed sinusoidal mode shapes $\phi_n(z) = \sin(k_n z + \varphi_n)$, we show that get $M_n = \rho AL/2$, where L is the total length of the beam. For each mode, the amplitude of the Bode plot,

$$\begin{aligned} \left|\frac{\phi_n(z_s)\phi_n(z_a)}{M_n((j\omega)^2 + 2\zeta_n\omega_n(j\omega) + \omega_n^2)}\right| &\le \frac{1}{2M_n\zeta_n\omega_n^2} \\ &= \frac{1}{\rho AL\zeta_n\omega_n^2}. \end{aligned} \tag{16}$$

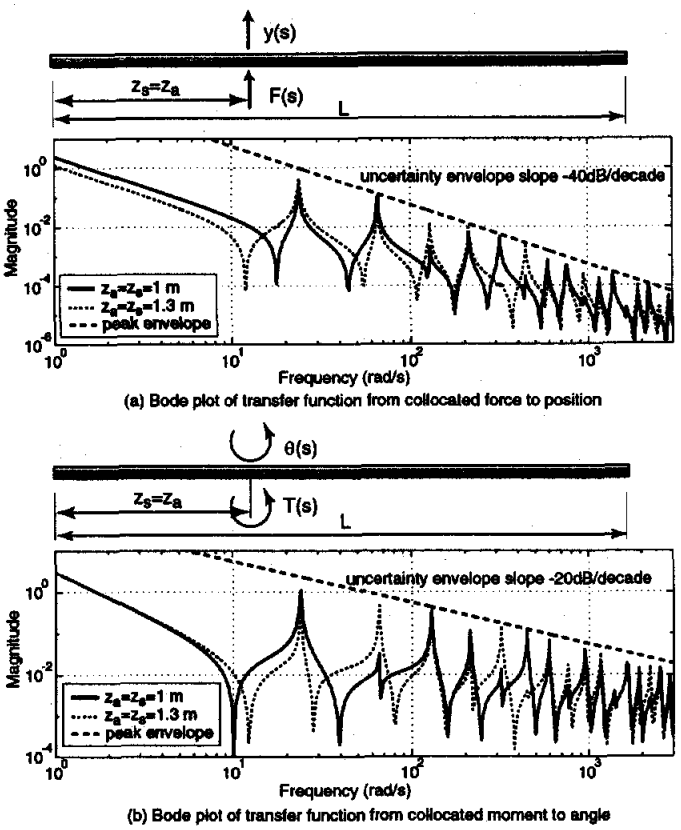

(a) Bode plot of transfer function from collocated force to position

(b) Bode plot of transfer function from collocated moment to angle

Fig. 2. Bode plots of transfer function $\frac{y(s)}{F(s)}$ vs $\frac{\theta(s)}{T(s)}$.

At each natural frequency, we assume that the corresponding resonance mode dominate and ignore the response from other modes, and if we assume the same ζ for each mode, then the peak envelope for the position control is:

$$\left|\frac{y(j\omega)}{F(j\omega)}\right| \le \frac{1}{\rho AL\zeta\omega^2}. \tag{17}$$

Similarly, the peak envelope of the transfer function for moment control can be derived as:

$$\left|\frac{\theta(j\omega)}{T(j\omega)}\right| \le \frac{k^2}{\rho AL\zeta\omega^2}. \tag{18}$$

Replacing the wave number k by frequency ω via (5) gives,

$$\left|\frac{\theta(j\omega)}{T(j\omega)}\right| \le \frac{1}{\sqrt{\rho AEI}L\zeta\omega}. \tag{19}$$

Comparing (17) and (19), the slope of the uncertainty envelope for moment control is -20dB/decade, while that of the position control is -40dB/decade as plotted in Fig. 2. So the moemnt/slope control is more challenging than the force/position control in [1] because the high frequency modes carry more amplitude and thus are harder to attenuate below 0dB.

FORCE/POSITION CONTROL

To control the position, we applied the averaging method of [1] to both sensors and actuators. As shown in Fig. 3, the average of two sensors' measurements is used to represent a single point's displacement. The averaged output $\hat{u}(z_o,t)$ is given by

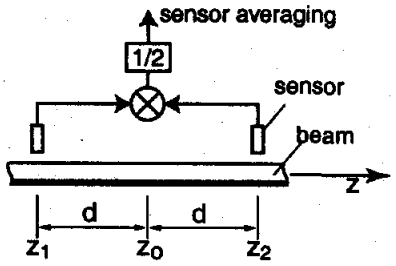

Fig. 3. Sensor positioning arrangement in 2-sensor averaging.

$$\begin{aligned}\hat{y}(z_o,t) &= \frac{1}{2}(u(z_1,t)+u(z_2,t)) \\ &= \frac{1}{2}\sum_{n=1}^{\infty}\xi_n(t)[\phi_n(z_1)+\phi_n(z_2)]. \quad (20)\end{aligned}$$

The averaged output of n-th mode is

$$\begin{aligned}\frac{1}{2}[\phi_n(z_1)+\phi_n(z_2)] &= \frac{1}{2}[C_{n1}(\cos k_n z_1+\cos k_n z_2) \\ &\quad +C_{n2}(\sin k_n z_1+\sin k_n z_2)] \\ &= (C_{n1}\cos k_n z_o + C_{n2}\sin k_n z_o)\cos k_n d \\ &= \phi_n(z_o)\cos k_n d, \quad (21)\end{aligned}$$

where $d = z_2 - z_0 = z_0 - z_1$. After placing this result into (20), the averaged output is

$$\hat{u}(z_o,t) = \sum_{n=1}^{\infty}\xi_n(t)\phi_n(z_o)\cos k_n d. \quad (22)$$

By averaging, a modal band-stop filter is created, where each mode has a gain of $\cos k_n d$. Fig. 4 shows the filter gain as function of wave number and frequency.

Actuator averaging is the dual to sensor averaging. As shown in Fig. 5, the simplest form of actuator averaging uses two actuators with the same force applied to each actuator. The resulting filtering effect is quite similar to sensor averaging. This idea can be understood via the concepts of modal force as described below. The averaged nth modal force N_n is given by

$$\begin{aligned}N_n &= \int_0^L f(z)\phi_n(z)dz \\ &= \int_0^L \frac{1}{2}\hat{f}(t)(\delta(z-z_1)+\delta(z-z_2))\cdot\phi_n(z)dz \\ &= \frac{1}{2}\hat{f}(t)(\phi_n(z_1)+\phi_n(z_2)) \\ &= \hat{f}(t)\phi_n(z_o)\cos k_n d. \quad (23)\end{aligned}$$

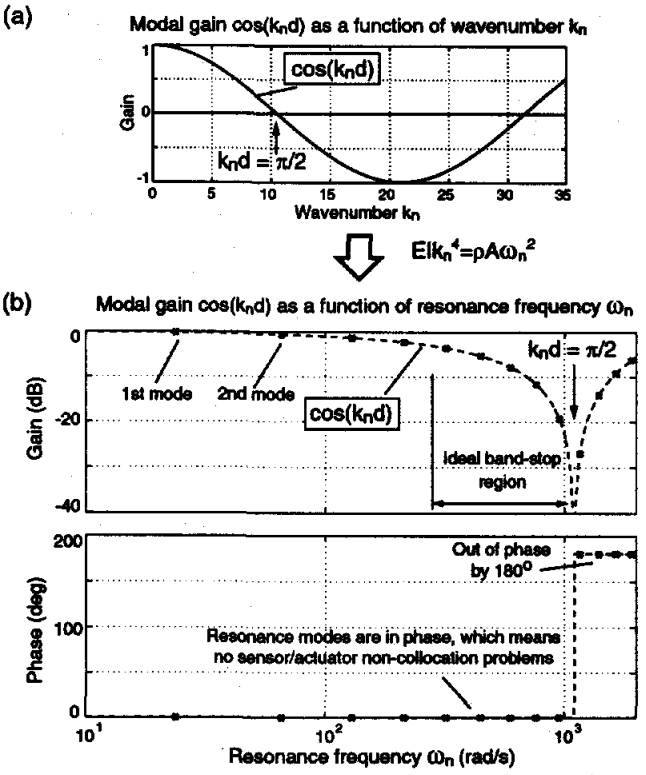

Fig. 4. 2-Sensor averaging for beams: modal gain $\cos k_n d$ plotted as (a) a function of k_n, and (b) a function of ω_n.

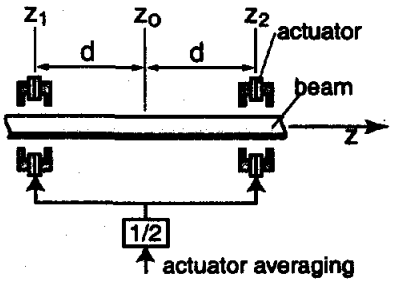

Fig. 5. Actuator positioning arrangement in 2-actuator averaging.

Here $\hat{f}(t)\phi_n(z_o)$ is the modal force associated with one actuator with force $\hat{f}(t)$ concentrated at $z = z_o$. The averaged modal force has a gain of $\cos k_n d$ just like the sensor averaging method.

With both sensor averaging and actuator averaging discussed above, the transfer function in one sensor/actuator set for force/position control becomes:

$$\frac{\hat{y}(s)}{\hat{f}(s)} = \sum_{n=1}^{\infty}\frac{\phi_n^2(z_o)}{M_n(s^2+2\zeta_n\omega_n s+\omega_n^2)}\cos^2 k_n d. \quad (24)$$

The resulting uncertainty envelope becomes:

$$\left|\frac{\hat{y}(j\omega)}{\hat{F}(j\omega)}\right| \le \frac{\cos^2 k_n d}{\rho A L\zeta\omega^2}, \quad (25)$$

which introduces a notch into the function (17)

MOMENT/SLOPE CONTROL

For two sensors set apart by a distance of $2d$ as shown in Fig. 6, the scaled difference $\hat{\theta}(z_0,t)$ of the two position sensor outputs is used to represent the rotation at the center point, and is given by

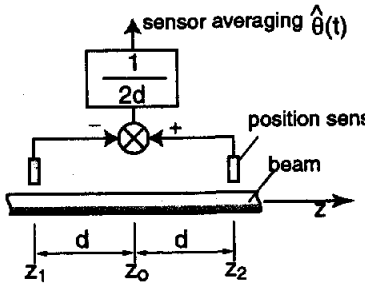

Fig. 6. Sensor positioning arrangement for moment/slope control.

$$\begin{aligned}\hat{\theta}(z_o,t) &= \frac{1}{2d}(u(z_2,t)-u(z_1,t)) \\ &= \frac{1}{2d}\sum_{n=1}^{\infty}\xi_n(t)[\phi_n(z_2)-\phi_n(z_1)]. \quad (26)\end{aligned}$$

The scaled deflection difference for the n-th mode is

$$\begin{aligned}\frac{1}{2d}[\phi_n(z_2)-\phi_n(z_1)] &= \frac{1}{2d}[C_{n1}(\cos k_n z_2-\cos k_n z_1) \\ &\quad +C_{n2}(\sin k_n z_2-\sin k_n z_1)] \\ &= \frac{1}{d}(-C_{n1}\sin k_n z_0+C_{n2}\cos k_n z_o)\sin k_n d \\ &= \frac{d}{dz}\phi_n(z_0)\frac{\sin k_n d}{k_n d} \\ &= \frac{d}{dz}\phi_n(z_0)\mathrm{sinc}(k_n d) \quad (27)\end{aligned}$$

After placing this result into (26), the averaged slope output is

$$\hat{\theta}(z_o,t)=\sum_{n=1}^{\infty}\xi_n(t)\frac{d}{dz}\phi_n(z_o)\mathrm{sinc}(k_n d). \quad (28)$$

By comparison with (3), we see that a modal band-stop filter is created again, where each mode is scaled by a gain of $\mathrm{sinc}(k_n d)$. Fig. 7 shows the filter gain as functions of wave number and frequency.

To demonstrate this "sinc" effect on the beam structure dynamics, the transfer function from an actuating moment $T(t)$ concentrated at z_0 to the averaging slope output $\hat{\theta}(t)$ $(=\frac{1}{2d}(u(z_2,t)-u(z_1,t)))$ centered on z_0 can be written by modal analysis as:

$$\frac{\hat{\theta}(s)}{T(s)}=\sum_{n=1}^{\infty}\left(\frac{\frac{d}{dz}\phi_n(z_o)\frac{d}{dz}\phi_n(z_o)}{M_n(s^2+2\zeta_n\omega_n s+\omega_n^2)}\cdot\mathrm{sinc}(k_n d)\right). \quad (29)$$

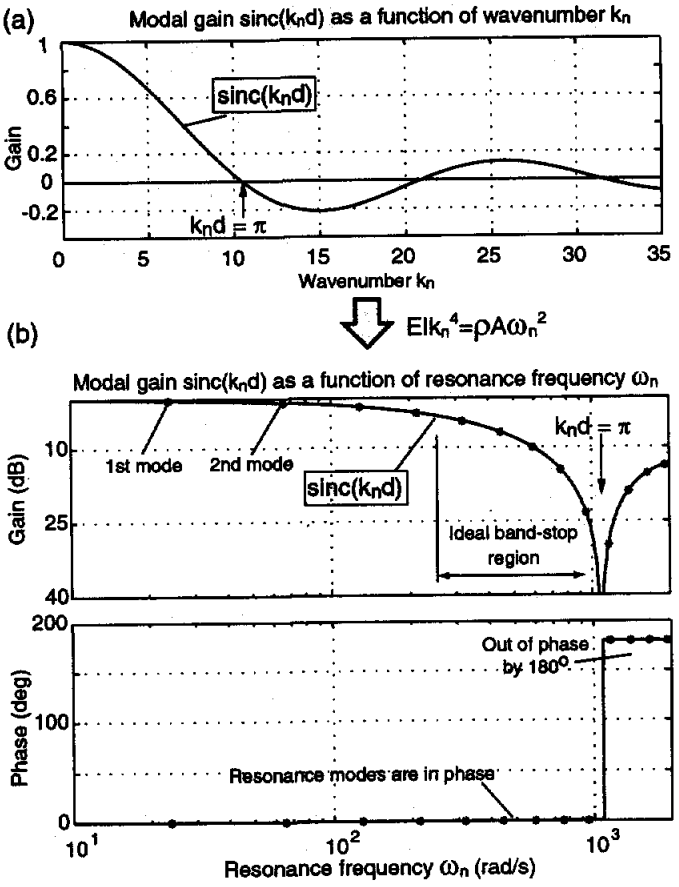

Fig. 7. 2-Sensor slope averaging for beam moment control: modal gain $\mathrm{sinc}(k_n d)$ plotted as (a) a function of k_n, and (b) a function of ω_n.

Compared with equation (15), the modal gain $\mathrm{sinc}(k_n d)$ in equation (29) attenuates the resonance modes over a broad range of frequencies without adversely affecting the phase. The Bode plot of this transfer function is shown in Fig. 8 for a free-free beam of length $L = 3$ m, sensor location $z_0 = 1$ m and spacing $d = 0.30m$.

The result (29) shows that spatial filter method for sensing slope yields a non-model-based modal-band-stop filter with the following properties:

1. It is independent of sensor pair location z_o.
2. It is independent of boundary conditions. When boundary conditions change, the natural frequencies associated with k_n change. That is, in Fig. 7, the curve remains the same, although the modes (shown as crosses) move along the curve.

Similar to the dual relation between sensor averaging and actuator averaging in force/position control, moment actuator averaging is the dual to slope sensor averaging. As shown in Fig. 9, the same forces but opposite direction are applied to each actuator. The nth modal force N_n associated with the differ-

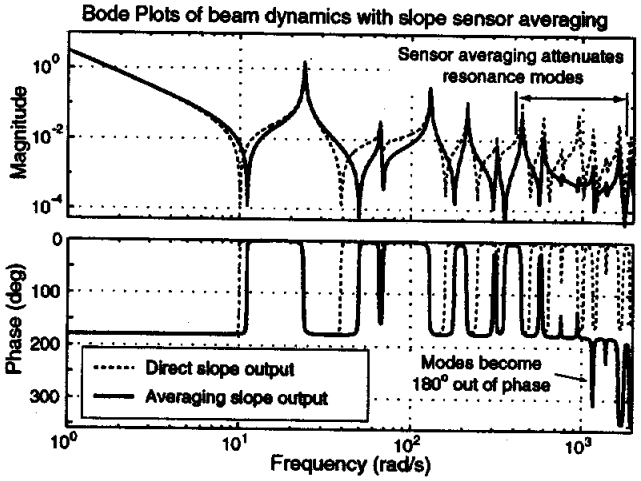

Fig. 8. Theoretical transfer function of beam model for slope sensor averaging. Solid line shows results with slope sensor averaging ($d = 30$ cm). Dashed line shows the transfer function from moment to collocated direct slope output for comparison. Note that a broad range of resonance modes are attenuated.

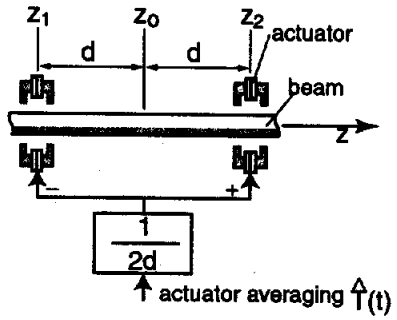

Fig. 9. Actuator positioning arrangement for moment/slope control.

ential force pair is given by

$$\begin{aligned} N_n &= \int_0^L f(z)\phi_n(z)dz \\ &= \int_0^L \frac{1}{2d}\hat{T}(t)(\delta(z-z_2)-\delta(z-z_1))\cdot\phi_n(z)dz \\ &= \hat{T}(t)\frac{1}{2d}(\phi_n(z_2)-\phi_n(z_1)), \end{aligned} \tag{30}$$

Plugging equation (27) into (30), we get

$$N_n = \hat{T}(t)\frac{d}{dz}\phi_n(z_o)\mathrm{sinc}(k_n d). \tag{31}$$

Compared with equation (13), $\hat{T}(t)\frac{d}{dz}\phi_n(z_o)$ is the modal force associated with one moment actuator with moment $\hat{T}(t)$ concentrated at $z = z_o$.

With both slope sensor averaging and moment actuator averaging discussed above, the transfer function in one sensor/actuator set for moment/slope control becomes:

$$\frac{\hat{\theta}(s)}{\hat{T}(s)} = \sum_{n=1}^{\infty} \frac{(\frac{d}{dz}\phi_n(z_o))^2}{M_n(s^2+2\zeta_n\omega_n s+\omega_n^2)}\mathrm{sinc}^2(k_n d). \tag{32}$$

The associated peak envelope becomes:

$$\left|\frac{\hat{\theta}(j\omega)}{\hat{T}(j\omega)}\right| \le \frac{k^2}{\rho AL\zeta\omega^2}(\frac{\sin k_n d}{k_n d})^2. \tag{33}$$

Fig. 10 shows the "sinc" effect on the Bode plots of the beam for moment/slope control. The "sinc"

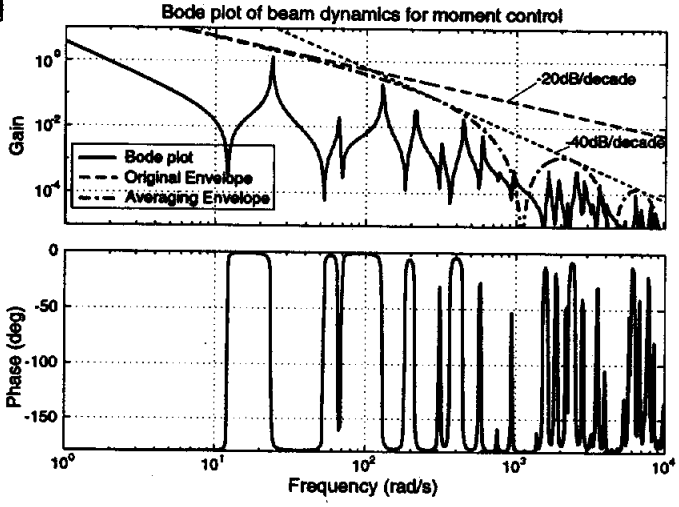

Fig. 10. Theoretical beam model with combination of sensor averaging and actuator averaging for moment control with $d = 0.30$m. The dotted line marked as -20dB/decade is the envelope without averaging. The dashed line is the envelope with sensor and actuator averaging. Note that the phase stays collocated above the notch as the result of the same spacing in sensor and actuator.

functions not only change the peak envelope for moment control from -20dB/decade to -40dB/decade, but also bring non-modal-based notches to the Bode plot. These effects will help us to increase the moment control bandwidth, and thereby stiffness significantly in the controller design.

CONTROLLER DESIGN

The challenges of controlling levitated flexible structures result from the following:

1. A levitated structure typically has a low damping ratio ζ, and the modes thus can have high peaks in the transfer function. In our experiment, we measure $\zeta \approx 0.001$ for free-free boundaries. This means that a very broad range of modes have an impact on loop stability.
2. Because of the sensor dynamics, actuator dynamics and computational and sampling time delay, the control systems usually have significant phase lag within the desired bandwidth.

3. As the suspended object is floating in the air, it will move axially relative to the actuator/sensor sets. As shown in Fig 2, the change in the actuator/sensor positions relative to the structure will influence the amplitudes of the resonance peaks greatly, and bring uncertainty to the controlled plant. As the magnetic suspension is applied to manufacturing processes, the boundary conditions will change significantly when the working piece is being cut or formed. The change in boundary conditions will move the natural frequencies and will bring further uncertainty to the plant.
4. Besides the robustness of the controller, we also want good performance of the magnetic suspension. We thus need high stiffness and damping to the magnetic bearing.

Taking advantage of the spatial filtering methods discussed above, we present a controller design method by loop compensation for the single moment/slope control first. Then, we extend it to the case where the levitated continua is controlled by both force/position and moment/slope sets.

Moment/Slope Loop Controller Design

Figure 11 shows the modelled plant dynamics from moment actuator and slope sensor with varied boundary conditions, including dynamics of the

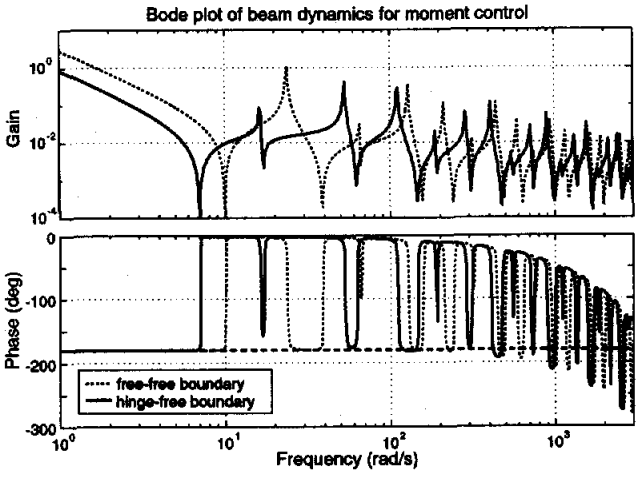

Fig. 11. Bode plots of open-loop dynamics, from collocated moment input command to a single slope sensor output voltage, including dynamics of beam, sensor, actuator and time delay, assuming damping ratio $\zeta = 0.005$

beam, actuator, sensor, and time delay (computational time of one sample and a half sampling time due to ZOH, the assumed sampling rate is 4kHz). This plant assumes a collocated slope sensor and moment actuator at $z_0 = 1$ m, for the experimental 3 m long beam. From the figure, it can be observed that the natural frequencies may change greatly with the boundary conditions.

In order to add positive phase to the modes over a broad frequency range, a multiple-lead slow-rolling compensator [1] is used to provide a phase margin of about 30 degrees for the frequencies of interest with an averaging gain slope of +1/2 in order to avoid over-amplifying resonance peaks at high frequencies. Nevertheless, the total phase of the loop transmission will fall below $-180°$ in the frequency range higher than a certain critical frequency ω_c, because the phase lag resulting from the actuator, sensor dynamics and computation and sampling time delays will be beyond the capability of lead compensators. At the frequency range $\omega \geq \omega_c$ where we cannot guarantee the phase greater than $-180°$, we need to attenuate the amplitude of the Bode plot of the loop transmission by the actuator averaging and sensor averaging methods discussed above so as to gain stability of the loop. The uncertainty envelope will be significantly attenuated by putting the averaging notch slightly less than the critical phase frequency ω_c. We adjust the controller gain to keep the peak envelope below -3dB at frequencies higher than the notching frequency ω_N and thereby assure stability. Fig. 12 shows the moment/slope compensation results with such spatial filters; the robust stability is

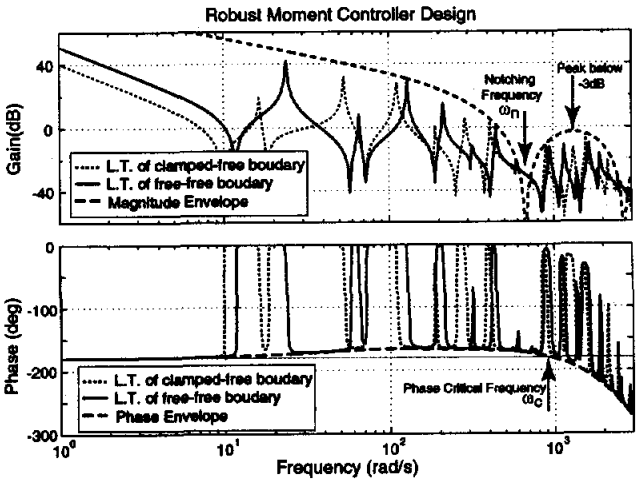

Fig. 12. Bode plots of loop transmission of moment control with spatial filtering methods. The dashed lines shows the magnitude envelope and phase envelope of the loop transmission.

easily verified because we compensate the loop based on the uncertainty envelope.

MIMO Combinational Control of Moment/Slope and Force Position

For the beam suspended by multiple sensor/actuator sets with both position and slope control, there will be strong interaction between the position control loops and slope control loops. The MIMO loop compensation of such a system is illustrated in Fig. 13. Here, we set the spacings in the slope control sets

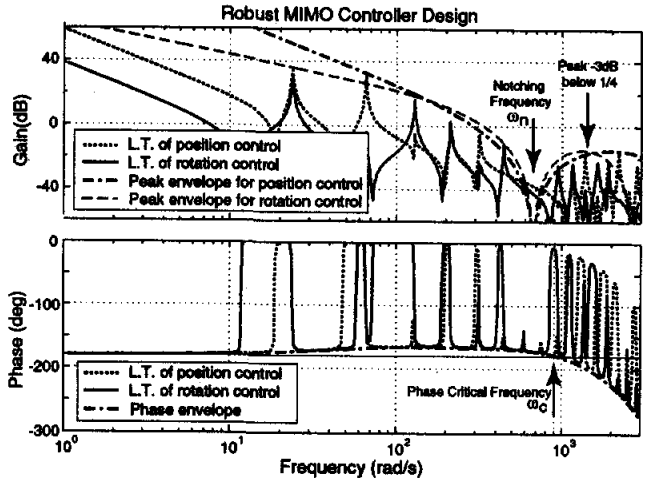

Fig. 13. Bode plots of loop transmission for rotation control and position control with averaging methods. The dashed lines shows the magnitude envelope and phase envelope of the loop transmission.

at two times that in the position control sets, so that all sets have the same notching frequency ω_N = 700rad/sec, which is slightly smaller than the critical phase frequency ω_c = 900rad/sec. The position controller and the slope controller have the same structure, *e.g.* the same poles and the zeros, as those in SISO moment controller. We adjust the gain of the controllers such that the loop transmission envelopes of both slope control and position control are -3dB below $1/n$, where n is the total number of sensor/actuator sets. Within the notching frequency ω_N, the phase envelope is always above $-180°$ because of the lead compensator. The peak envelope and the phase envelope remains the same regardless of the boundary conditions and positions of sensor/actuator sets, thus robust stability is guaranteed.

EXPERIMENTAL RESULTS

In this section, we show experimental results from our scaled tubular beam magnetic suspension.

Experimental Setup

In our experiment, both sensors and actuators have 12.7 mm bores, their design is discussed in [10], [11]. The tube is steel, with a mass per unit length ρA = 0.1190 Kg/m, Young's Modulus E = 200 GPa, outside diameter ϕ = 6.35 mm, wall thickness w = 0.89 mm, and length L = 3 m. The experiment controller is implemented on a digital signal processing (DSP) board with a sampling time of 250 μs. Total computational time within this sampling interval is about 235 μs.

Moment Control of Clamped-clamped Beam with Spatial Filtering

To verify the effectiveness of slope/moment control with spatial filtering, we use 2 sensors and 2 actuators to implement this experiment. Specifically, the space between sensors is 0.80 m, the space between actuators is 0.70 m, and the center point of the sensors coincides with that of the actuators. Fig. 14 shows the experimental setup and the measured loop transfer function. First, we put the set at a relatively

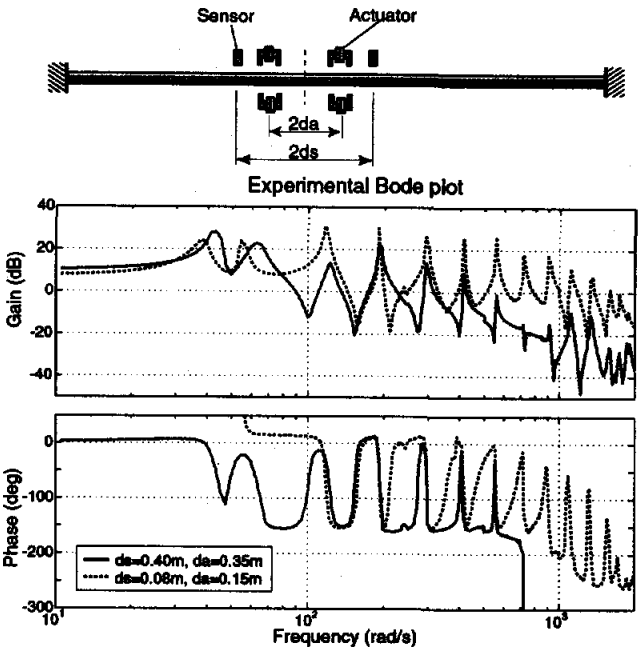

Fig. 14. Experimental setup and measured Bode plots of loop transfer function for moment control by using 2-actuator averaging and 2-sensor averaging and with clamped/clamped boundary conditions.

wide spacing d_s = 0.40m and d_a = 0.35m. The corresponding notches are at around 600 rad/s and 800 rad/s. We compensate the loop as in previous section. This is a stable result. Next, we put the set at narrower space d_s = 0.08m and d_a = 0.15m; the corresponding notching frequencies are above 4000rad/s and have no significant filtering effect in the frequency range of Fig. 14. When closing the loop with the same controller as above, the plant is unstable with a loop transmission as shown with the dashed line in Fig. 14. The closed loop plant remains unstable until the controller gain is reduced by a factor of 10. This means that with the spatial filtering effects, the stiffness (controller gain) can be made larger by a factor of 10.

MIMO Force/Position and Moment/Slope Control of Free-free Beam

While the tubular beam is being suspended with free-free boundaries, the damping ratio of the beam is measured to be below 0.001. As shown in Fig. 15, we use three sensor/actuator sets for position con-

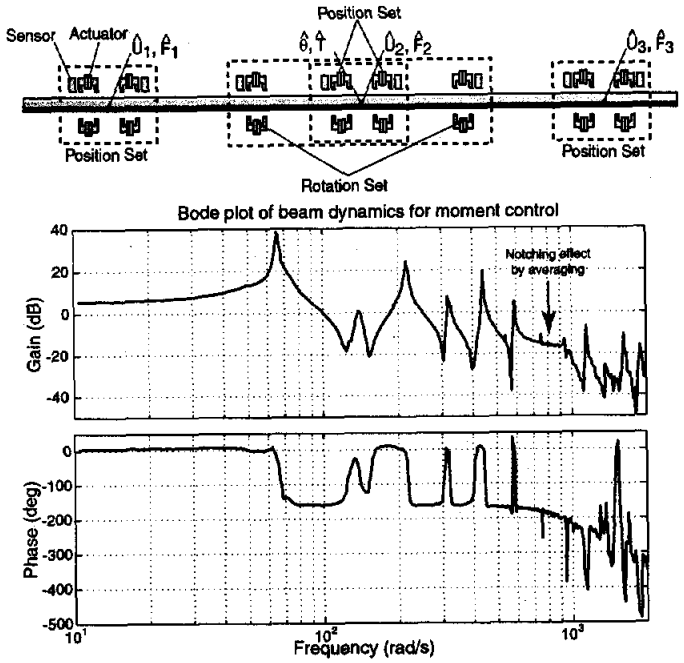

Fig. 15. Experimental setup and Bode plots of moment control loop transmission at the 2nd point with all loops closed using both sensor averaging and actuator averaging.

trol at points 1, 2 and 3 and one sensor/actuator set for slope control at point 2 to suspend the beam. The mid-point of the rotation set coincides with that of the second position set. In the position sets, the spacing between two sensors/actuators are $2d_s = 0.355$ m and $2d_a = 0.275$ m, which set the associated "cosine" filter notches at 775 rad/sec and 1340 rad/sec. In the slope set, the spacing between the two sensors $2d_s = 0.710$ m and the spacing between two actuators $2d_a = 0.610$ m, which sets the associated "sinc" filter notches at 775 rad/sec and 1000 rad/sec. Because of the physical size of our self-developed sensors and actuator, we can not make the spacing between two sensors equal to that between two actuators in one set. The experimental setup and measured Bode plots of the loop transmission at the moment/slope control loop with all other loops closed is shown in Fig. 15. It can be observed that there are obvious notching effect at 770 rad/sec by spatial filtering. The phase for the frequency range below 700 rad/sec is above $-180°$. Beyond this frequency range, we attenuate the peak envelope of amplitude below 0 dB.

CONCLUSIONS

This paper presents the spatial filtering technique for combined force/position and moment/slope control of levitated continua. This spatial filtering method makes use of the relations between resonance frequencies and wavelengths as they depend on structural properties. By placing sensors and actuators based on the wavelengths of undesired modes, we can attenuate these resonance modes to improve the loop gain. These filtering effects is both mathematically analyzed and experimentally demonstrated. As the resulting modal gain is independent both of sensor/actuator set location and of boundary conditions, a robust controller can be designed with the envelope information to deal with the uncertainty coming from the changes in position and boundary conditions. Furthermore, this filtering technique can be widely extended to vibration control of other flexible structures such as filaments, webs and plates. The main limitation of our analysis is that we assume sinusoidal modal shapes, and thus neglect the evanescent waveforms. This assumption is acceptable when the sensors and actuators are far from the boundaries of a slender suspended member. The approximation is especially applicable at high frequencies where the wavelengths are short. The resulting analytical simplification allows the development of powerful spatial filtering concepts, which appear to have wide applicability.

REFERENCES

[1] M. C. Weng, X. Lu and D. L. Trumper, "Magnetic Suspension of Flexible Structures for Non-Contact Processing," in *Proc. of the 7th Int. Symp. on Magnetic Bearings*, ETH Zurich, Switzerland, Aug. 23-25, 2000.

[2] Y. Oshinoya and T. Shimogo "Electro-magnetic Levitation Control of an Elastic Plate," in *Proc. Maglev '89*, pp. 435-440, 1989.

[3] H. Hayasiya, H. Ohsaki, and E. Masada "Magnetic Levitation Control of Elastic Steel Plate for Steel Making Process," in *Proc. ICEE '95*, 1995.

[4] J. Jin, T. C. Yih, T. Higuchi, and J. U. Jeon, "Direct Electrostatic Levitation and Propulsion of Silicon Wafer," *IEEE Trans. Industry Applications*, vol. 34, No. 5, pp. 975-984, 1998.

[5] American Metal Handle, Vulcan Dr., Birmingham, AL, USA.

[6] Yohji Okada, Kumiko Shimizu, and Satoshi Ueno, "Vibration Control of Flexible Rotor by Inclinaation Control Magnetic Bearings with Axial Self-Bearing Motor," *IEEE/ASME Trans. on Mechatronics*, vol. 6, No. 4, pp. 521-524, 2001.

[7] B. Wie, "Active Vibration Control Synthesis for the Control of Flexible Structures Mast Flight System," *Journal of Guidance*, Vol. 11, No. 3, pp. 271-277, 1988.

[8] M. J. Balas, "Active Control of Flexible Systems," *Journal of Optimization Theory and Applications*, Vol. 25, No. 3, pp. 415-436, 1978.

[9] L. Meirovitch, *Elements of Vibration Analysis*, Chapter 5, McGraw-Hill, 1975.

[10] D. L. Trumper, M. C. Weng, and R. J. Ritter, "Magnetic Suspension and Vibration Control of Beams for Non-contact Processing," in *Proc. IEEE CCA-CACSD '99*, pp. 551-557, 1999.

[11] M. C. Weng, and D. L. Trumper, "A Design Method for Magnetic Suspension and Vibration Control of Levitated Beams for Non-contact Processing," in *Proc. NASA ISMST-5 '99*, 1999.